Bollettino di Geofisica Teorica ed Applicata Vol. 61, n. 4, pp. 589-606; December 2020
DOI 10.4430/bgta0326

Design and implementation of a marine seismic source by electrical discharge

A. Giordano[1], L. De Luca[1] and P. Giordano[2]

[1] *Università degli Studi Parthenope, Napoli, Italy*
[2] *Università degli Studi Federico II, Napoli, Italy*

(Received: 23 October 2019; accepted: 6 April 2020)

ABSTRACT Acoustic sources based on electrical discharge, commonly called sparker sources, are employed in surveys for high-resolution marine stratigraphy. In this work, a new seismic sparker-type transducer has been designed, built and tested to obtain specific characteristics: low cost, small size (50×50×15 cm^3), high resolving power, perfect symmetry of the acoustic beam emitted, and high directivity. This source can, thus, also be used in shallow water, to delineate the first sedimentary layers. First, an analysis of the determined experimental radiation pattern, signal to noise, and wavelet shape is presented. The radiation pattern is subsequently compared to the theoretical one. Lastly, comparative tests with traditional sparker sources and with the boomer source showed the validity of the performance of the new source.

Key words: sparker, boomer, seismic profiles, radiation pattern.

1. Introduction

At the University "Parthenope" of Naples, there are currently electro-acoustic instruments for the investigation of the seabed, such as the EG&G (1977) sparker[1], the M.E.A.S. (Multispot Extended Array Sparker) (Mirabile *et al.,* 1991), the Sam96 (Giordano *et al.,* 2003), and the boomer (EG&G International Inc., Boomer seismic profiling system, Waltham, MA, USA). However, during recent years, research is heading towards the study and implementation of sea stratigraphy at medium and low depth, for applications in marine construction such as dams, bridges and jetties and in the field of geological, archaeological, and environmental research.

On this basis, considerable focus has been given to electric low-cost sources with low power consumption, which can be safely and quickly installed and used. The great advantage of such sources is that their power supply systems are easily manageable, thus allowing their transport on small boats and their operation in shallow water, in proximity of beaches, coasts and ports.

The aim of this research is to have a high signal - to - noise ratio (SNR) of the acoustic new source and, moreover, to improve the concentration of the radiated energy in a very narrow solid angle, in order to obtain the ensonification of a smaller surface of the bottom of the sea (the footprint) (Clay and Medwin, 1977; Verbeek, 1992). This procedure reduces the intensity of the

[1] The sparker is a seismic source, discovered in 1956 by S.T. Knott and J.B. Hersey; when a high-voltage electric discharge is rapidly generated through an electrode (wire) immersed in salt water, it produces a bubble of ionised gas, which by expansion creates an acoustic wave, able to penetrate hundreds of metres of sediments.

© 2020 – OGS

echoes coming from other directions. Thus, the new source has a higher directivity and a higher vertical resolving power (*VRP*[2]) (Widess, 1982; McGee, 2000) than the boomer source (Edgerton and Hayward, 1964; Simpkin, 2005), regarded as the standard instrument in the field of marine stratigraphy.

The *VRP* equation is:

$$VRP = \left(\frac{v \cdot \tau}{2} \right) \tag{1}$$

where v is the speed of sound in water and τ is the duration (ms) of the pulse emitted from the source (acoustic signature).

In order to obtain this directive system, we have implemented an array source, which has the advantage of reducing the secondary periodic oscillations, and is also characterised by a very narrow pulse (De Vita *et al*., 1979; Mirabile *et al*., 1991; Giordano *et al*., 2003).

The homebuilt source (Figs. 1 and 2) consists of a 10×10 square matrix, equal to 100 copper electrodes 30 cm long, with a distance between them of about 0.02 m, arranged on a square support of 50 cm per side. The 100 electrodes are powered in phase and a square grid functions as the electric ground.

Fig. 1 - Detail of the homebuilt prototype: the electrodes are clearly visible.

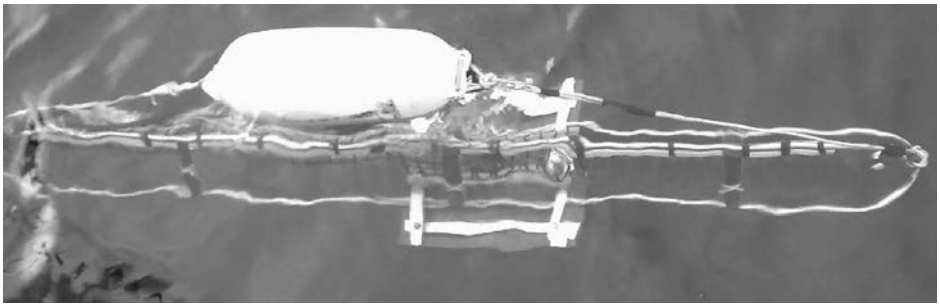

Fig. 2 - The new source at sea during the test phases.

[2] The *VRP* expresses the capacity to discriminate two contiguous reflectors on the vertical plane.

To estimate the radiative parameters and to study their behaviour, the source has been experimentally tested both in the time domain for the evaluation of the signature (pulse duration) and in the frequency domain (frequency spectrum).

2. Experiment: radiation pattern

The radiation pattern of the new transducer was determined through a series of measurements, carried out in the open sea (see the Appendix). The following elements have been used for the acquisition of data:

- power supply EG&G;
- trigger capacitor bank;
- new transducer (square array);
- reference hydrophone;
- filter bank band-pass (Kron-Hite) (0.2/20,000 Hz; -12 dB);
- DSeismic software (Corradi *et al*., 2004).

The measurements were done so as to avoid reflection, refraction and diffusion of the signals by the reflective surfaces along the path source-receiver (e.g. the support boat).

The acquired signals are direct measurements, affected only by minimal attenuation due to propagation. Furthermore, it is assumed that the chemical composition of the sea, temperature and pressure are constant in the column of water from 0 to -10 m.

The acquisition was done through a reference hydrophone with omni-directional characteristics of the Bruel&Kjaer mod. 8100, with reference sensibility (RS) of -205.7 dB - to 1V/μPa ±3 dB up to a frequency of 100 kHz (Fig. 3).

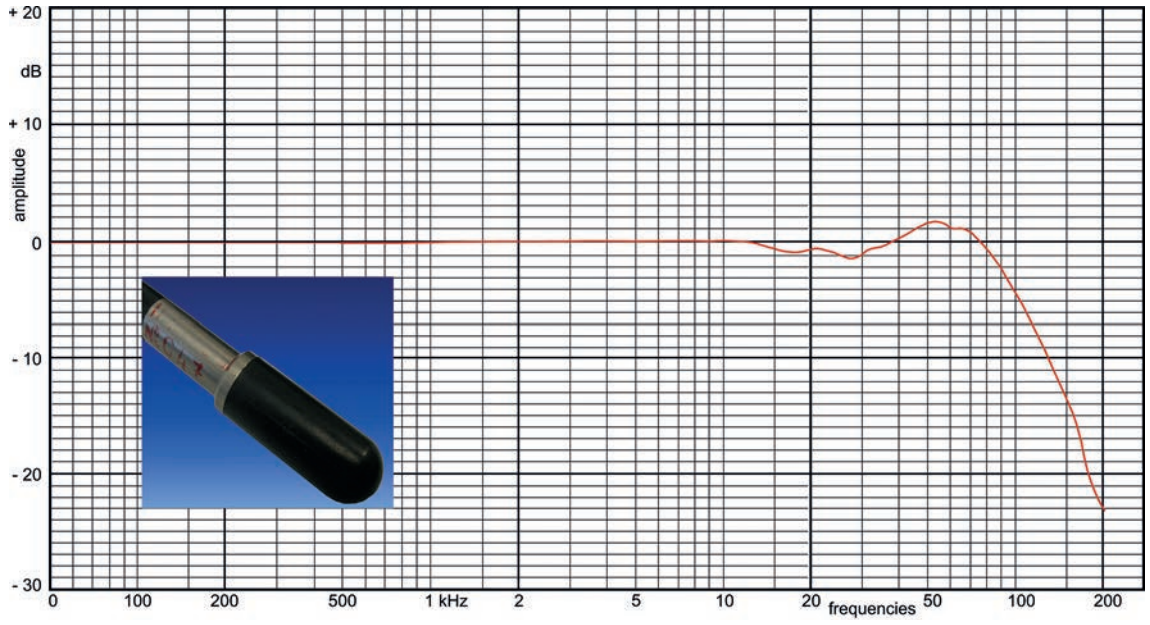

Fig. 3 - Reference hydrophone used for measurements; the band extends from 0 to 100 kHz.

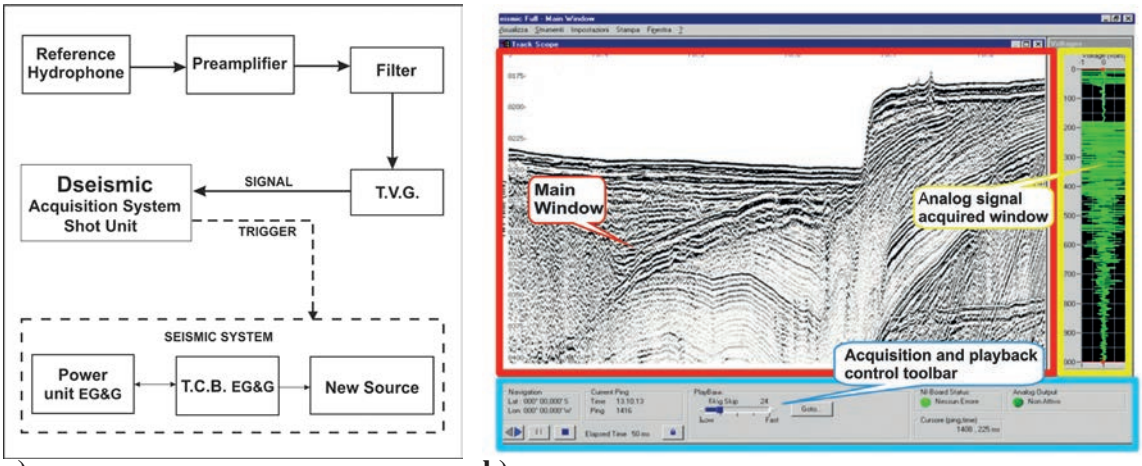

Fig. 4 - DSeismic acquisition system: a) block diagram; b) main window.

The signals have been acquired and processed with DSeismic (Giordano *et al*., 2002, 2003; Corradi *et al*., 2004), a software developed at the Parthenope University of Naples (Italy) in the frame of the PNRA project (National Research Project in Antarctica). DSeismic works in a Windows environment, allowing both the acquisition and the playback of the already acquired seismic lines. The main window is shown in Fig. 4b.

DSeismic allows to perform a real-time analysis of the FFT (Fast Fourier Transform) frequency spectrum on the acquired seismic signals. The block diagram in Fig. 4a shows the signal path. The analogue signal coming by the hydrophone passes within a broadband preamplifier. Data are sampled with a National Instrument board, "PCI 6014 to 16 bit", whose sampling frequency is fc = 200 kHz, installed in a PC with Intel Pentium processor. The signal passes through a 10 to 6000 Hz band-pass filter, in order to avoid aliasing.

The source has been powered by an EG&G (Fig. 5) system, made up of a power supply and a trigger capacitor bank, with an energy of 200 J, using an electric generator of 4.5 kW.

Six measurements were made at the distance of 1 m and 3 m horizontally at various depths (0.2, 2, 4, 6, 8, 10 m), according to the geometry of Fig. 6. The distribution of this field is a function of the elementary contributions of the

Fig. 5 - Power system EG&G, mod. 231-232.

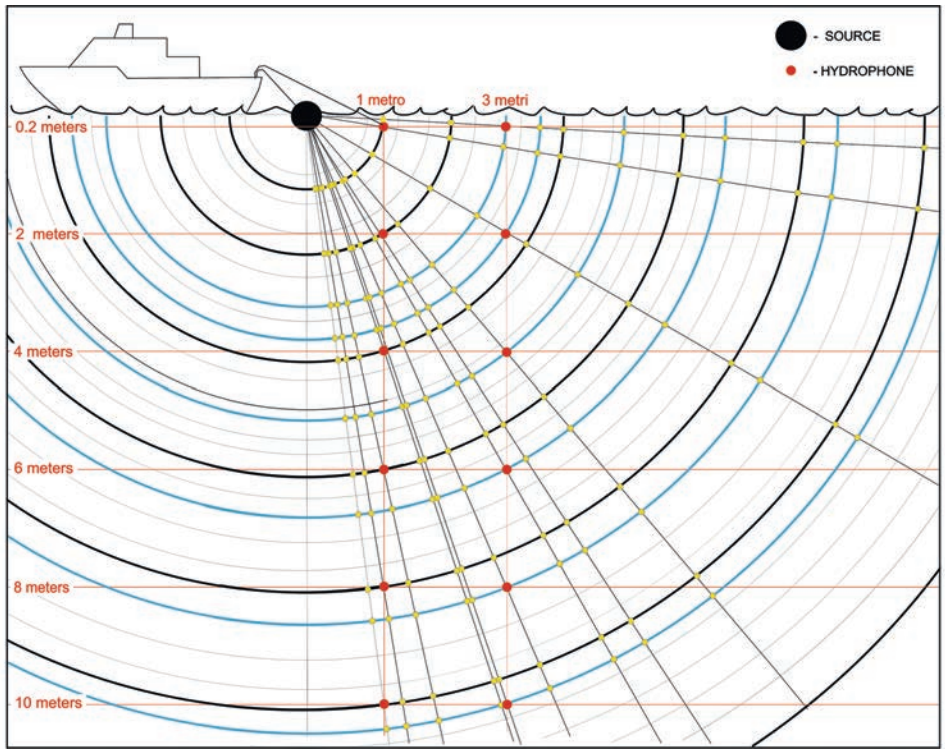

Fig. 6 - Geometry used for the acquisition in the "far field" end of the direct rays from the source to the hydrophone.

various electrodes that make up the source (Urick, 1979). They produce significant variations in amplitude and phase of the signals (see the Appendix).

The intensity of the received signals are expressed in terms of pressure; the relationship between acoustic intensity and pressure is:

$$I = \frac{P^2}{2\rho v} = \frac{P^2}{2Z} \tag{2}$$

where: P is the sound pressure, ρ the density of the medium, v the speed of sound in water, Z the acoustic impedance.

The intensity of radiation is a function of θ and r:

$$I = I(\theta, r). \tag{3}$$

In quantitative terms, the propagation of sound in fluids is described by the wave equation. The intensity of sound in any medium decreases with distance from the source, a phenomenon defined as transmission loss. In general, this loss is composed of two elements: loss for spreading and absorption. With the assumption of homogeneous medium, the energy radiated from the source spreads in all directions with spherical symmetry, as $1/r^2$, where r is the radial distance between the emitter and the receiver. In our case, with the hypothesis of far field, the space of measurements is confined between two planes, the sea surface and the sea floor, and the signal acquired decreases with the law $1/r$.

Along the path, the energy generated from the source undergoes progressive attenuation due to the friction within the medium, which leads to energy loss in the form of heat. The energy loss E_{loss} for absorption and spreading is determined by:

$$E_{loss} = 0.5 \cdot \rho \cdot f^2 \cdot I^2 \tag{4}$$

where: f is the frequency, I the intensity of radiation and ρ the density of the material. The set of the two phenomena is is highlighted by the following equation:

$$I(r) = I_0 \frac{r_0}{r} e^{(-\alpha r)} \qquad \text{for } r_0 < r \tag{5}$$

where the term $1/r$ takes into account the effect of the spherical divergence, while the exponential term is constrained by the absorption, I_0 is the reference radiation intensity to the distance r_0, α is the sea water attenuation coefficient. For every angle θ, applying Eq. 5 we have derived 12 measurements of the radiation intensity, obtaining a 12×12 matrix, where each row contains the measurements of radiation intensity on a given radius circumference (Fig. 6).

Table 1 shows:

- the depth of the various measurements in metres (column 1);
- the radial distances (real distance source-hydrophone) to 1 and 3 m horizontally (columns 2 and 5);
- the intensity of radiation (Sound Pressure Level - SPL_{dB}) (columns 3 and 6);
- the angles of incidence (columns 4 and 7).

Table 1 - Measures made at various depths.

Depth (m)	Radial distance to 1 m (horizontal)	Radiation intensity SPL_{dB}	Degree angles	Radial distance to 3 m (horizontal)	Radiation intensity SPL_{dB}	Degree angles
0.2	1.02	157	79°	3.10	14	87°
2	2.24	135	30°	3.60	25	57°
4	4.12	69	15°	5.00	60	37°
6	6.12	98	10°	6.74	51	29°
8	8.10	83	8°	8.54	61	21°
10	10.04	44	6°	10.44	29	16°

3. Comparison of the theoretical and experimental radiation patterns

The signature of a seismic source is composed of a main pulse followed by various oscillations, with periods that depend on the type and size of the source and the energy used. These oscillations are considered inconvenient, since they increase the pulse duration, thereby decreasing the resolving power (*VRP*). *VRP* of space-time reaches its maximum when the duration of the pulse (the signature) approaches the Dirac pulse.

In the traditional sparker sources, the signature has a duration of about 1.2 ms (Mirabile, 1969; Le Tirant, 1976; Jones, 1999), with the presence of substantial oscillations, as it is shown in Fig.

7a. Consequently, the resolution is very low and, by applying Eq. 1, *VRP* ~ 0.9 m. This value is not suitable to distinguish the surface layers of the sea bottom, as Table 2 shows.

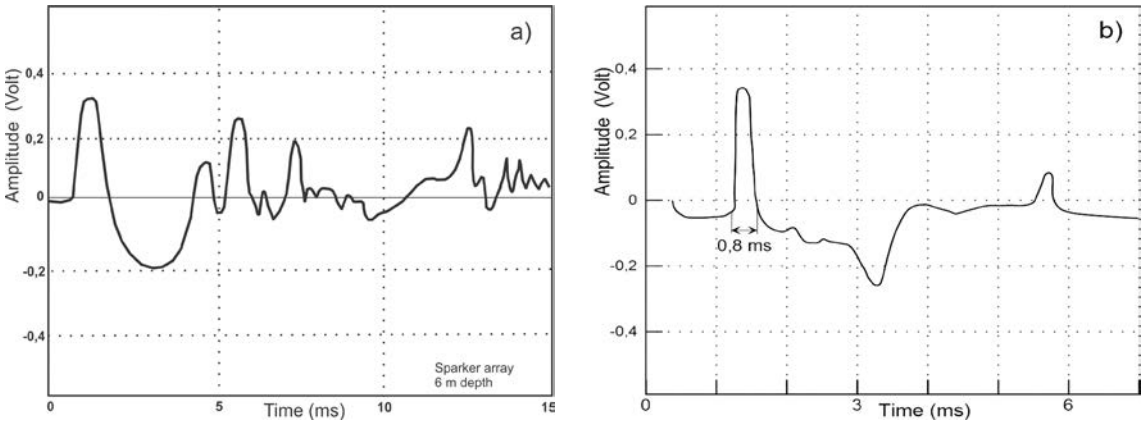

Fig. 7 - a) Signal of a traditional sparker-array source with three-electrodes. b) Signal of a boomer source.

Fig. 7b shows the signature of the boomer source, which is significantly smaller than the sparker signature. Fig. 8 shows a series of signatures of our transducer, which, for simplification, we will call Square due to its peculiar shape, acquired at various depths. The good repeatability of the signatures is clearly shown.

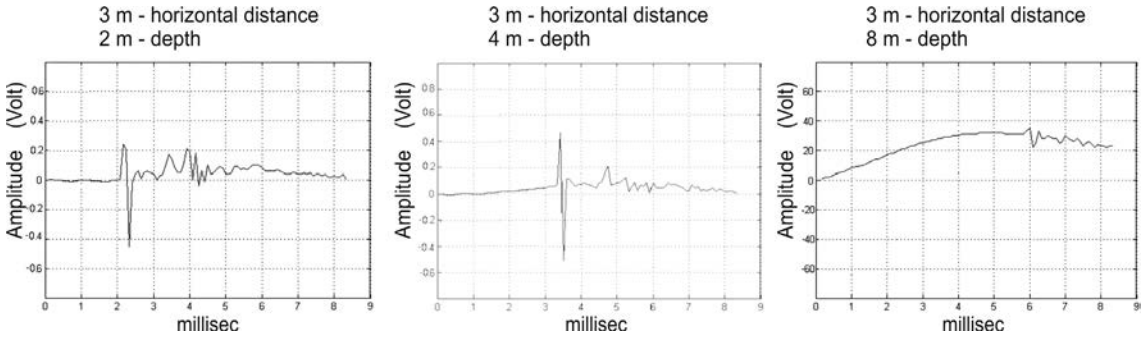

Fig. 8 - Square signatures at various depths.

The signature of the Square is comparable to the signature of the boomer source. As a matter of fact, the duration of both signatures is almost identical (Table 2).

Fig. 9 shows a zoomed view of a generic acquired signature: besides the primary impulse, we note that secondary, quickly dampening, pulses are present. In fact, our "Square" has a very narrow acoustic signature in the time domain, which is fundamental in determining the *VRP* (Widess, 1982). To determine the radiation pattern, we processed the direct signals according to the geometry in Fig. 6, at a depth of about 6 m, regarded as the optimal depth of work in our area of interest.

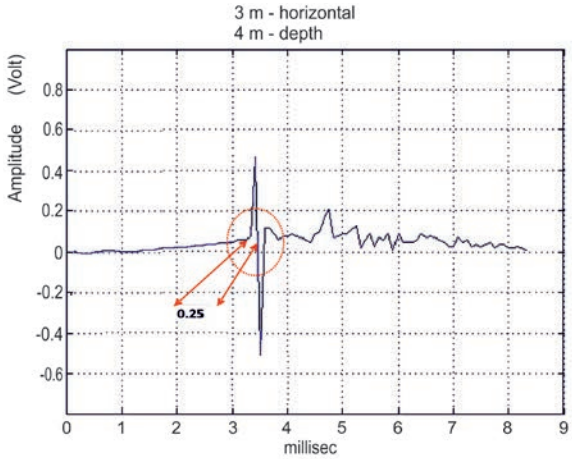

Fig. 9 - Direct signal received by the hydrophone at 4 m of depth. Power emitted: 200 J.

Table 2 - Comparison of characteristics between sources.

	New Source (Square)	Boomer	Sparker
Power (J)	200	200	200
Signature τ (ms)	0.25	0.80	1.20
Spectrum (Hz)	20-3000	100-3000	20-700
Shooting cadence (s)	0.50	0.50	0.50
Resolution (*VRP*) (m)	0.18	0.15	0.90
Dimensions	0.50×0.50×0.15	1.60×0.90×0.60	2.00×0.30×0.30
Weight (Kg)	15	90	35

Table 2 shows a comparison of characteristics between the Square, the boomer, and the sparker sources. The advantages of the Square are, in addition to its *VRP*: low realisation cost, small size, and low weight.

With an estimated signature duration *t* of 0.25 ms (duration of the 1st peak, in the dashed area in Fig. 9), Eq. 1 gives a *VRP* of about 18 cm. Moreover, from the spectral analysis in Fig. 10, we note the presence of significant energy between 50 and 700 Hz with further information at higher frequencies, up to about 3 kHz.

The fundamental feature, highlighted in this work, is the directivity of the Square, whose footprint at a depth of 6 m is very narrow compared to the boomer source.

Fig. 11 shows the experimental polar plot, which has been obtained from the calculation of the experimental measurements,

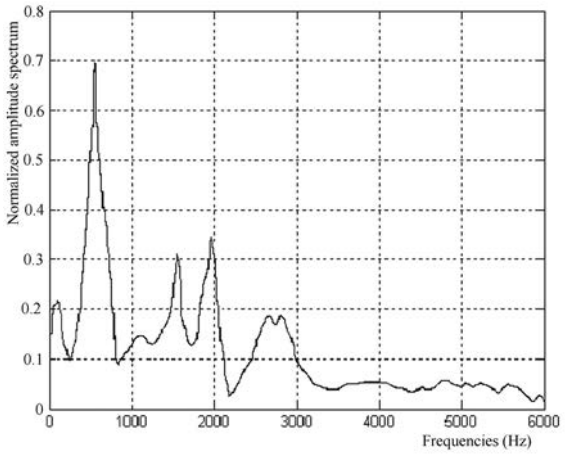

Fig. 10 - Amplitude spectrum of the direct signal, up to about 3000 Hz.

normalised at the maximum value. By comparing the theoretical radiation diagram (Fig. 12), obtained using Eq. A14 (see the Appendix), with the experimental one, it is possible to notice that the behaviour of the Square comes near to the theoretical prediction (Buogo and Cannelli, 1999). The symmetry conditions have been taken into account.

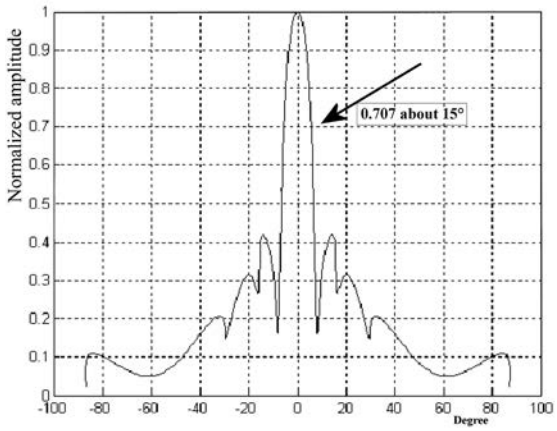

Fig. 11 - Normalised experimental polar plot: the solid angle is approximately 15°.

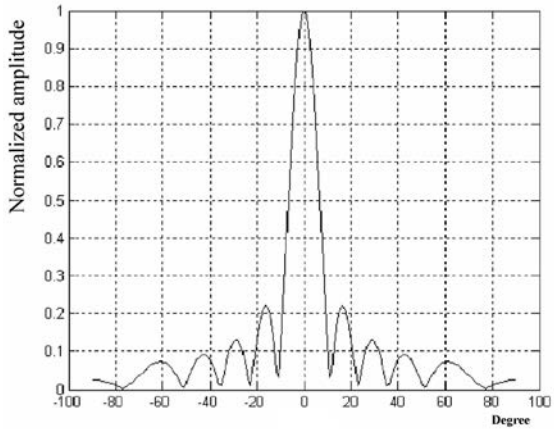

Fig. 12 - Theoretical directional response, obtained using Eq. A14.

The radiation beam width, which is the measurement of the solid angle Ω centred on the axis of radiation, where the majority of emission energy is concentrated, can be seen in Fig. 11. It is approximately 15°, close to the theoretical value obtained using Eq. A8 (De Dominicis Rotondi, 1990; Verbeek and McGee, 1995):

$$\Omega(\varphi = 0°) = \arcsin\left(\frac{\lambda}{(N+1)d}\right) \cong 14° \tag{6}$$

where: λ (about 0.5 m) is the wavelength at the maximum frequency of the amplitude spectrum, N is the total number of the electrodes equal to 100 and d is the distance between the electrodes, equal to 0.02 m.

In quantitative terms, the value of the directivity is expressed by the Directivity Index (*DI*):

$$DI = 10\log\left(\frac{I_d}{I_a}\right) \tag{7}$$

equal to the ratio of the intensity of the acoustic field, I_d and I_a, in logarithmic units (Brekhoskikh, 1960). In our case, for the Square, most of the energy is concentrated in the solid angle Ω, therefore the directivity can be approximately expressed as:

$$DI = 10\log\left(\frac{4\pi}{\Omega}\right). \tag{8}$$

For a solid angle of 15°, which equals to $\pi/12$ rad, we have:

$$DI = 10\log\left(\frac{4\pi}{\left(\frac{\pi}{12}\right)^2}\right) \cong 23dB\,. \tag{9}$$

From Eq. A10 (see the Appendix) the result in absolute value is:

$$\frac{I_d}{I_a} = 10^{\frac{DI}{10}} \cong 200 \tag{10}$$

from which:

$$I_d = 200 I_a. \tag{11}$$

Therefore, we demonstrated that our source has the expected higher directivity.

Fig. 13 represents the polar pattern and its volumetric field of radiation, obtained from the experimental measures.

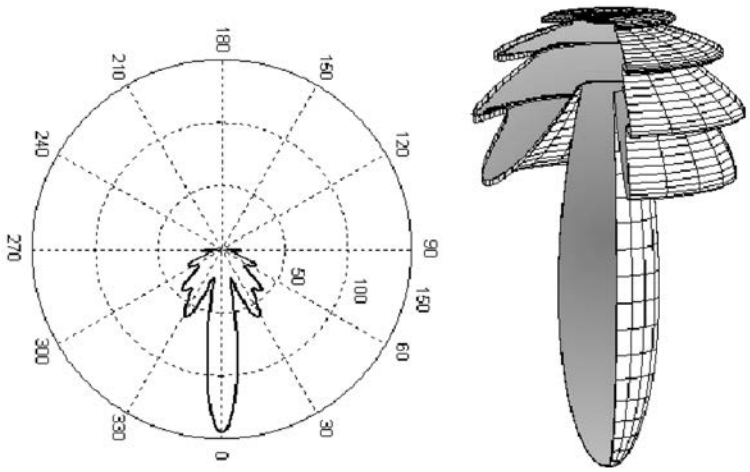

Fig. 13 - The polar plot and its three-dimensional polar response of experimental measurements.

4. Comparative tests

A seismic line has been acquired on the field with the Square in the Pozzuoli Bay. A comparative test has been performed between this line and two lines of the boomer source (L_P1 and L_Porto2) acquired in the same area.

The EG&G boomer source has been used as an acoustic source for the realisation of seismic profiles in deep and shallow water for over forty years and has a reputation for reliability, high resolution, adaptability, fidelity, and ease of use. It is an electromagnetic system, which EG&G developed in the 1960s, consisting of a plate of resin (Fig. 14) with a copper coil (inductance), on which an aluminium plate with a diameter of about 0.5 m is mounted through a spring system. When the copper coil is traversed by the impulsive current, magneto-motor forces (eddy currents)

are generated in the aluminium plate that moves away against the force of spring, due to the electromagnetic repulsion effect. This instantaneous movement creates a cavitation bubble in the sea which subsequently implodes, generating a pressure wave.

The energies emitted from the boomer range from 200 to 500 J and significantly have a spectrum up to about 7000 Hz, with the maximum energy emitted around 3000-3500 Hz.

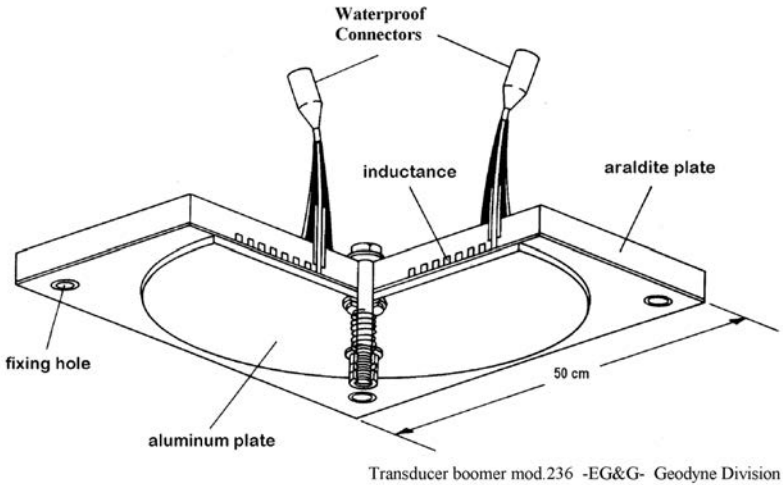

Fig. 14 - Boomer: araldite base with aluminium plate (Edgerton and Hayward, 1964).

The lines used for the tests are shown in the navigation plan in Fig. 15: Square4 line about 500 m long, L_P1 line about 435 m long, L_Porto2 line of about 325 m in length. The pier visible in the plan is about 220 m long.

From the seismic profile of L_P1 line (Fig. 16) we note that, at about 260 m from the beginning of the line, a lateral echo is present due to the base of the pier (Fix3-4). On the Square4 line, around the Fix5, the lateral echo of the pier is absent. This section of the seismic profiles corresponds to the area of interest in the dotted circle (Fig. 15).

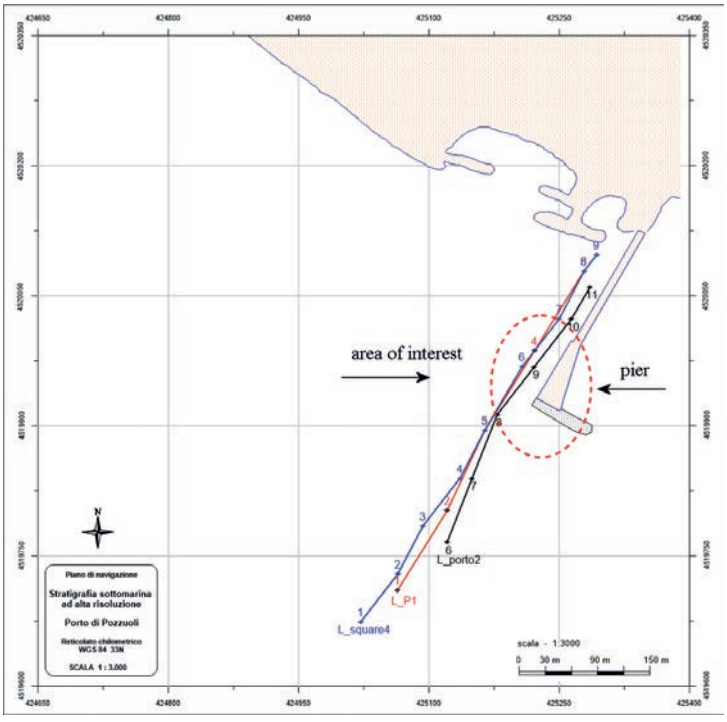

Fig. 15 - Navigation map of seismic lines recorded in the Pozzuoli Bay.

The absence of the echo proves that the Square source is very directive, which means it has a very narrow footprint on the seabed.

In the line realised with the Square source, a high resolution and a good SNR is evident and this allows discriminating a higher number of seismic reflectors in the first 30 ms of penetration in the marine sea bottom (Mc Quillin *et al*., 1979).

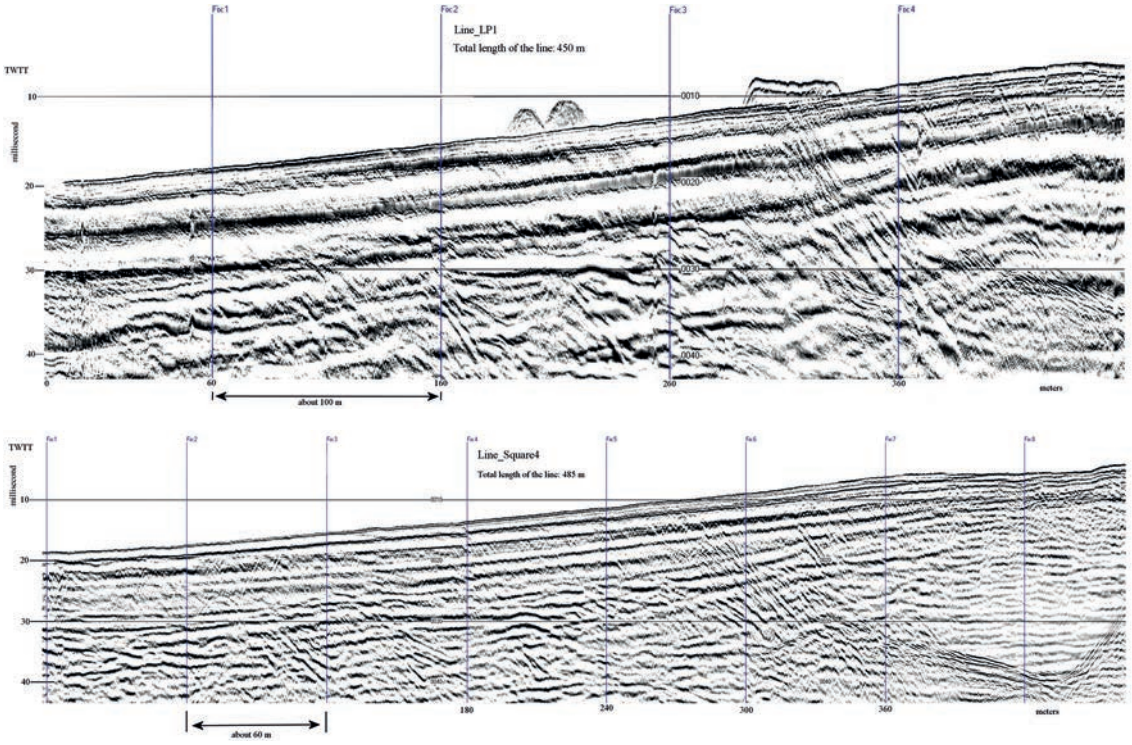

Fig. 16 - Seismic profiles: L_P1 line vs L_Square4 line - Pozzuoli Bay.

To further confirm the higher directivity of the Square, we have considered a third line (L_ Porto2), made with the boomer source. On this line, there is still a lateral echo due to the base of the pier, around 150 m (Fix8 and Fix9 in Fig.17) taking into account that on the navigation plan in Fig. 15, the L_Porto2 line starts from Fix6.

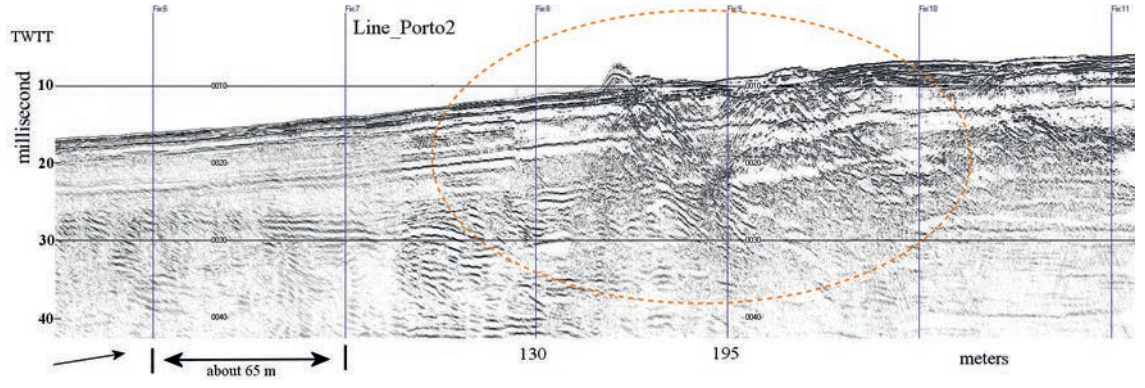

Fig. 17 - Seismic profile: L_Porto2 line. Test area in the dotted circle. Pozzuoli Bay.

Lastly, Fig. 18 shows the difference between the Square line and the sparker Line 22_90[3]. The sparker is a source of depth, characterised by a spectrum oriented towards low frequencies. It has a low resolution in the first layers of the sub-basement. The Square, instead, has a finer resolution in such layers.

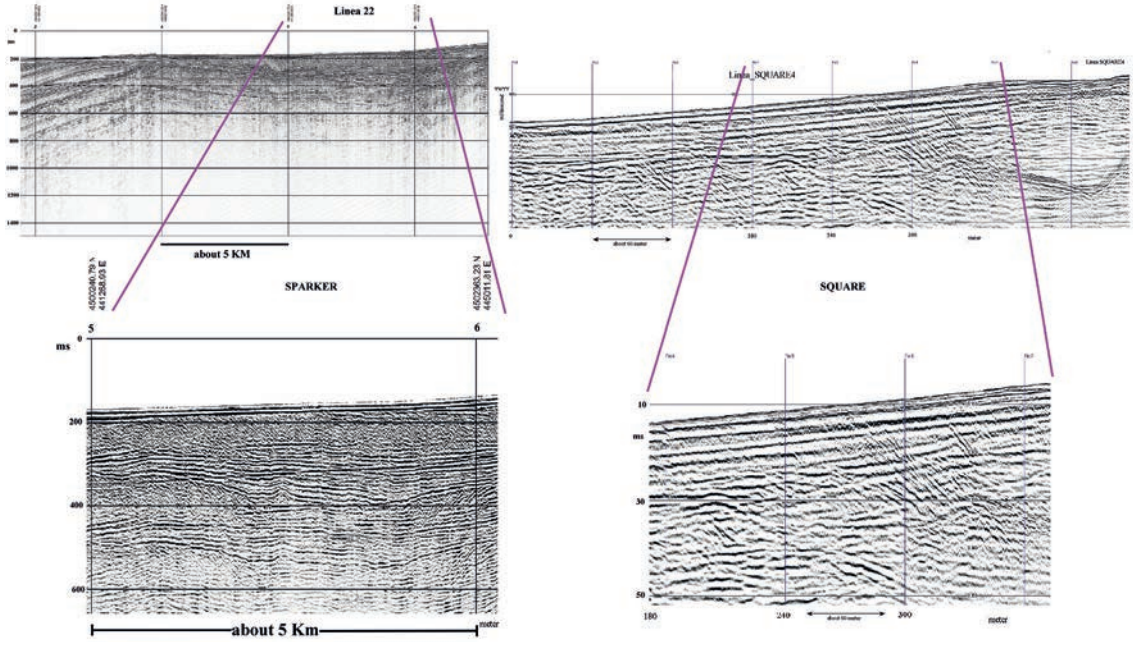

Fig. 18 - Comparison between the L_22_90 sparker line and the L_Square4 - Pozzuoli Bay (Gulf of Naples).

5. Conclusion

The tests carried out at sea have proved that the Square is a seismic source with high resolution, high SNR, and high directivity. Its performance is comparable to the one of the boomer EG&G seismic source, considered an ideal source to survey the first sedimentary layers of the seabed.

The Square has a very compact size and requires simple steps to mount. Furthermore, it is low-cost and the control system of the electrodes is very fast and easy to use.

During the working phases, it was found that the consumption of the electrodes is about 1 cm/h at an energy of 200 J and a shooting cadence of 0.5 s. These are remarkable features, since the repeatability and stability of the generated signal (signature) depend on these parameters. The Square, thus, proved to be particularly suited for seismic explorations in shallow water and allows working in restricted areas along the coast for the discrimination of the first sedimentary layers. Fig. 19 shows a detail of the L_Square4 line, with a magnification in the dashed box. About 80 m are approximately displayed horizontally. In the surface layers, we note thicknesses in the order of 0.1 ms, corresponding to about 0.15 m (using an acoustic velocity of 1500 m/s).

[3] The L_22_90 line and the L_Square4 line were made by the University of the Parthenope Studies, Geophysics section, in the Gulf of Napoli.

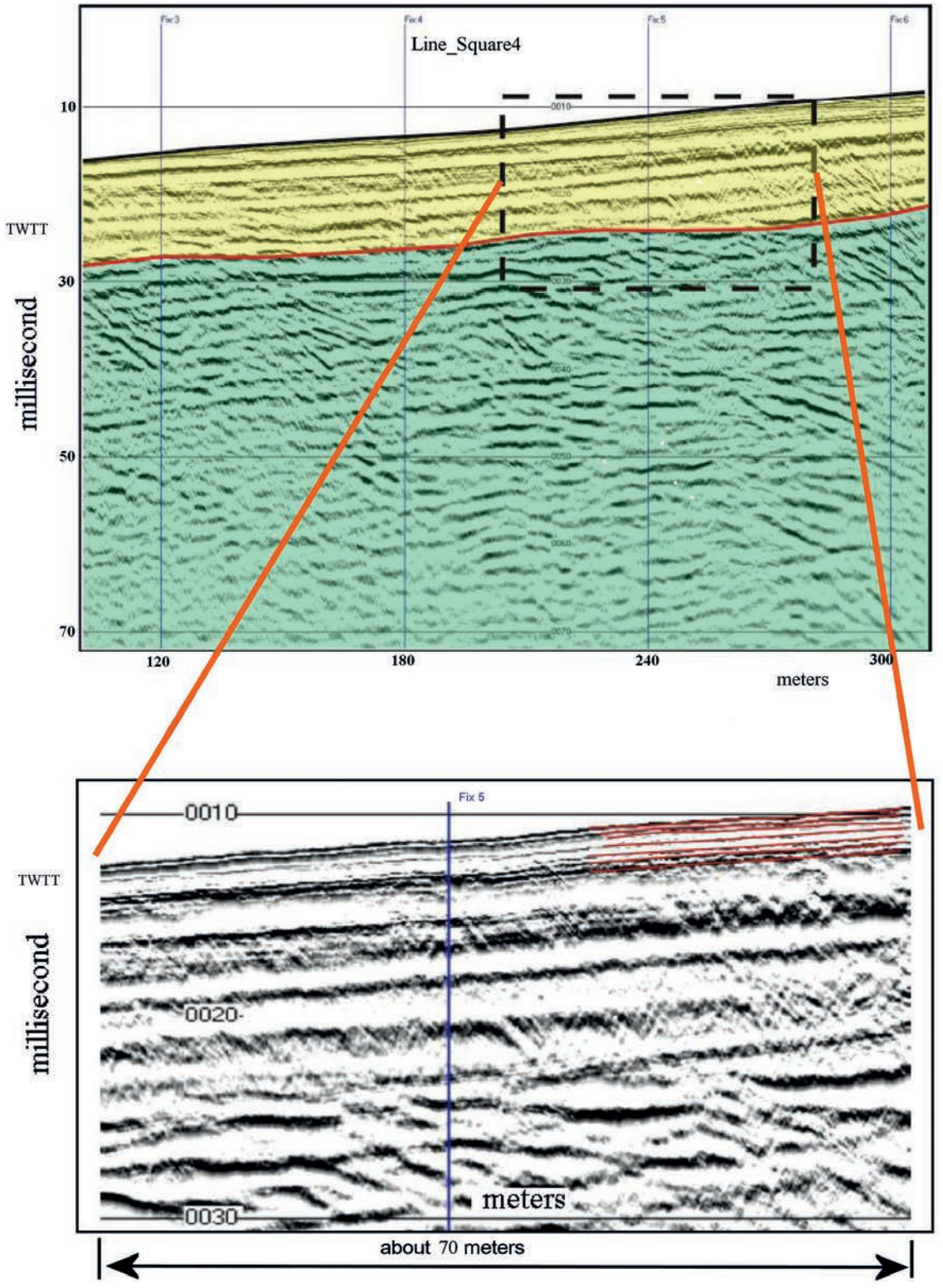

Fig. 19 - Detail of a portion of the L_Square4 line. In the upper layers of the sediments we note thicknesses in the order of 0.1 ms equal to about 15 cm, highlighted in red. Pozzuoli Bay.

Acknowledgements. We are grateful to prof. Lorenzo Mirabile for founding in the 1970s a research group who has stimulated our intelligence in the study of underwater electroacoustic. In addition, the writers thank Claudia De Luca for her kind availability, for her help, suggestions and support provided for the realisation of the relative manuscript.

REFERENCES

Brekhoskikh L.M.; 1960: *Waves in layered media*. Academic Press, New York, NY, USA, 561 pp., ISBN 0-12-30560-0.

Buogo S. and Cannelli G.B.; 1999: *Source level and directivity pattern of an underwater pulsed sound generator based on electrical discharge*. Acoust. Lett., **23,** 54-59.

Clay C.S. and Medwin H.; 1977: *Acoustical oceanography: principles and applications*. Wiley&Sons, New York, NY, USA, 562 pp.

Corradi N., Giordano F. and Giordano R.; 2004: *The application of a very high resolution hardware and software (D-Seismic) system for the loss of seismic data for the study of the Ross Sea sedimentary*. In: Atti, Associazione Italiana Oceanologia Limnologia, Genova, Italy, vol. 17, pp. 115-124.

De Dominicis Rotondi A.; 1990: *Principi di elettroacustica subacquea*. ELSAG Spa, Genova, Italy, vol. 1, pp. 89-93.

De Vita S., Esposito B. and Mirabile L.; 1979: *Criteri di progetto di sparker a cortina per sismica ad alta risoluzione*. In: Atti, Convegno Scientifico Nazionale Progetto Finalizzato Oceanografia e Fondi Marini, CNR, Roma, Italy, 5-7 ottobre 1979.

Edgerton E.H. and Hayward G.G.; 1964: *The 'boomer' sonar source for seismic profiling*. J. Geophys. Res., **69**, 3033-3042, doi: 10.1029/JZ069i014p03033.

EG&G; 1977: *Sparker source systems*. Marine Instruments Brochure, Gaithersburg, MD, USA, Bullettin 2-100 A.

Giordano F., Giordano R. and Corradi N.; 2002: *D-Seismic: a very flexible low cost hardware/software system for acquisition, real time and post processing of seismic data of Ross Sea (Antartica 2002 expedition)*. In: Proc., Forum ACUSTICUM, Seville, Spain, 7 pp., <www.sea-acustica.es-43.40.Ph.001>.

Giordano F., Giordano R., Corradi N., Nicotra G., Ortosecco I. and Pittà A.; 2003: *Improving "S/N" in reflection seismic marine records by mean SAM96 (Sparker array multitip) and D-Seismic (hardware - software system for seismic data acquisition and processing*). In: Poster, 5th European Conference on Noise Control, EURONOISE 2003, Naples, Italy, n. SC39-389.

Jones E.J.W.; 1999: *Marine geophysics*. Wiley&Sons Ltd, Chichester, UK, 466 pp., doi: 10.1016/S0025-3227(00)00033-5.

Le Tirant P.; 1976: *Reconnaissance des sols en mer pour l'implantation des ouvrages pètroliers*. Pubblication de l'Institut Francais du Petrole. Scienze et Technique du Petrole, N°21, 114 pp.

McGee T.M.; 2000: *High-resolution seismic profiling on water*. Ann. Geophys., **43**, 1045-1073, doi: 10.4401/ag-3688.

McQuillin R., Bacon M. and Barcly W.; 1979: *An introduction to seismic interpretation, 1st ed*. Grahm&Trotman Ltd, London, UK, 199 pp.

Mirabile L.; 1969: *Prime esperienze di stratigrafia sottomarina eseguite presso l'Istituto Universitario Navale*. Ann. IUN, **XXXVIII**, 30 pp.

Mirabile L., Fevola F., Galeotti F., Ranieri G. and Tangaro G.; 1991: *Sismica monocanale ad alta risoluzione con sorgente multispot di tipo Sparker: applicazione ai dati di tecniche di deconvoluzione*. In: Atti, 10° Convegno Annuale Gruppo Nazionale Geofisica della Terra Solida, Roma, Italy, pp. 431-444.

Orfanidis S.J.; 2004: *Electromagnetic waves and antennas*. Online book, Rutgers University, New Brunswick, NJ, USA, <www.ece.rutgers.edu/~orfanidi/ewa/>.

Rayleigh J.W.S.; 1945: *The theory of sound, 2nd ed*. Courier Dover Publications, New York, NY, USA, 480 pp.

Simpkin P.G.; 2005: *The Boomer sound source as a tool for shallow water geophysical exploration*. Mar. Geophys. Res., **26**, 171-181.

Urick R.J.; 1979: *Sound propagation in the sea*. The University of Michigan, Ann Arbor, MI, USA, 300 pp.

Verbeek N.H.; 1992: *Directivity of high-resolution marine sources*. In: Weydert M. (ed), Proc. 1st European Conference on Underwater Acoustics, Luxembourg, pp. 644-647.

Verbeek N.H. and McGee T.M.; 1995: *Characteristics of high-resolution marine reflection profiling source*. J. Appl. Geophys., **33**, 251-269.

Widess M.B.; 1982: *Quantifying resolving power of seismic system*. Geophys., **47**, 1160-1173, doi: 10.1190/1.1441379.

Corresponding author: Alberto Giordano
DIST - Centro Direz. Is. C4, Università degli Studi Parthenope
Via Acton 38, 80133 Napoli, Italy
Phone: +39 081 5476668; e-mail: alberto.giordano@uniparthenope.it

Appendix: Radiation field of a discrete source

The radiation field of a discrete source is divided into two main regions called: near field region and far field region (De Dominicis Rotondi, 1990; Orfanidis, 2004). The near field extends up to a distance r from the radiator equal to:

$$r = \lambda/2\pi \tag{A1}$$

where λ is the wavelength.

The distribution of this field is a function of the elementary contributions due to the various electrodes that make up the source, which produce significant variations in amplitude and phase of the signals.

In the far field, the contribution of the difference between the amplitudes tends to shrink, as $1/r$, while the phase differences vary significantly with the angle θ (Figs. A1 and A2).

The far field begins at a distance called Fraunhofer distance, which provides the limit between the near and far field:

$$r = 2D^2/\lambda \tag{A2}$$

where D is the largest dimension of the radiator.

The generation of acoustic energy of a discrete source is closely related to the compression and decompression of steam bubbles formed near the electrodes (Mirabile, 1969).

The distribution of the radiation field is the sum of the contributions of the electrodes that make up the radiator. In the far field, $r \rightarrow \infty$, the pressure waves emitted from two adjoining elements in the array (Fig. A1) interfere with each other in a constructive way in a preferential direction, producing significant changes in amplitude and phase, due to the path difference:

$$\Delta r = d \cdot \sin\theta \tag{A3}$$

where d is the distance between two electrodes and θ is the incidence angle.

In point P (Fig. A1), the path difference creates delays proportional to this difference, introducing a phase difference on each harmonic of the spectrum:

$$\Delta\varphi = k \cdot \Delta r \tag{A4}$$

where k is the wave number.

This results in a deformation of the resulting signal due to the phase distortion φ. The maximum value of $\Delta\varphi$ admissible to the phase shift expresses

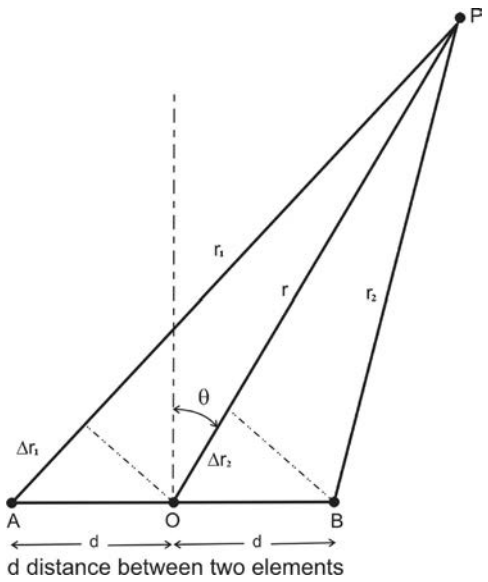

Fig. A1 - Linear geometry between two electrodes.

the "sinphasic condition". For this value we must refer to the maximum significant frequency of the signal spectrum, to which corresponds the value of the minimum wavelength λ_{min}, which determines the minimum distance that can be distinguished in the vertical plane, independently of the verified "sinphasic condition". Our source can be considered as a discrete plane array consisting of elementary sources powered all in phase, equally spaced and aligned.

In Fig. A2, *dx* and *dz* are the distances between the contiguous elements, *mdx* and *ndz* are the coordinates of each element with *m* and *n* integers.

The field radiated by the generic element (monopole) at a point P to infinity, will be given by the following expression (Rayleigh, 1945; De Vita *et al.,* 1979; De Dominicis Rotondi, 1990):

$$P(r,t,\theta,\varphi) = \frac{A}{r} e^{j(\omega t - kr)} \tag{A5}$$

where: *A* is a constant, calculated using the conditions to the limit, with:

$$r = r_1 + \Delta r \quad \text{and} \quad \Delta r = \bar{O}C \cdot \sin\theta. \tag{A6}$$

Exploiting Δr you have:

$$\Delta r = (m \cdot dx \cdot \cos\varphi + n \cdot dz \cdot \sin\varphi) \cdot \sin\theta \tag{A7}$$

by taking into account the components along the *x* and *z* axis of the $\bar{O}C$ segment. The pressure is the total sum of all contributions of individual primary elements:

$$P(r,t,\theta,\varphi) = \sum_{m=\frac{-M}{2}}^{\frac{M}{2}} \sum_{n=\frac{-N}{2}}^{\frac{N}{2}} P_i(r,t,\theta,\varphi). \tag{A8}$$

On axis *y*, with $\theta = 0°$ the pressure is expressed by:

$$P\,(r,t,\theta,\varphi) = P_a\,(\theta = 0) \cdot F\,(\theta,\varphi) \tag{A9}$$

where $F\,(\theta, \varphi)$ is the directional response (or directivity factor) (De Dominicis Rotondi, 1990), and is equal to:

$$F(\theta,\varphi) = \frac{I_d(\theta,\varphi)}{I_a(\theta,\varphi)} \tag{A10}$$

where $I_d\,(\theta, \varphi)$ is the radiation intensity of a real source, while $I_a\,(\theta, \varphi)$ is the intensity of radiation of isotropic source of equal power.

For a source of $M \times N$ electrodes, it is given by the following equation:

$$F(\theta,\varphi) = \frac{1}{(M+1)(N+1)} \left[\frac{\sin\left[k\left(\frac{M+1}{2}\right) dx \sin\theta\cos\varphi\right]}{\sin\left[k\frac{dx}{2}\sin\theta\cos\varphi\right]} \right] \cdot \left[\frac{\sin\left[k\left(\frac{N+1}{2}\right) dx \sin\theta\cos\varphi\right]}{\sin\left[k\frac{dx}{2}\sin\theta\cos\varphi\right]} \right]. \tag{A11}$$

$F\,(\theta, \varphi)$ on the axis y has unit value:

$$\lim_{\theta \to 0} F(\theta, \varphi) = 1. \tag{A12}$$

Then, from Eq. 7 it is reduced:

$$P(r, t, \theta, \varphi) = P_a(\theta = 0) \tag{A13}$$

In our case, with $M = N$ and $dx = dz = d$, the directivity factor in the plane of symmetry for an angle $\varphi = 0°$ (or $\varphi = 90°$) becomes:

$$F(\theta) = \frac{1}{(N+1)^2} \left\{ \frac{\sin\left[\frac{\pi(N+1)}{\lambda} d \sin\theta\right]}{\sin\left[\frac{\pi}{\lambda} d \sin\theta\right]} \right\}^2 \tag{A14}$$

while in the plane diagonal for angle $\varphi = 45°$ it is:

$$F(\theta) = \frac{1}{(N+1)^2} \left\{ \frac{\sin\left[\frac{\pi(N+1)}{\sqrt{2}\lambda} d \sin\theta\right]}{\sin\left[\frac{\pi}{\sqrt{2}\lambda} d \sin\theta\right]} \right\}^2. \tag{A15}$$

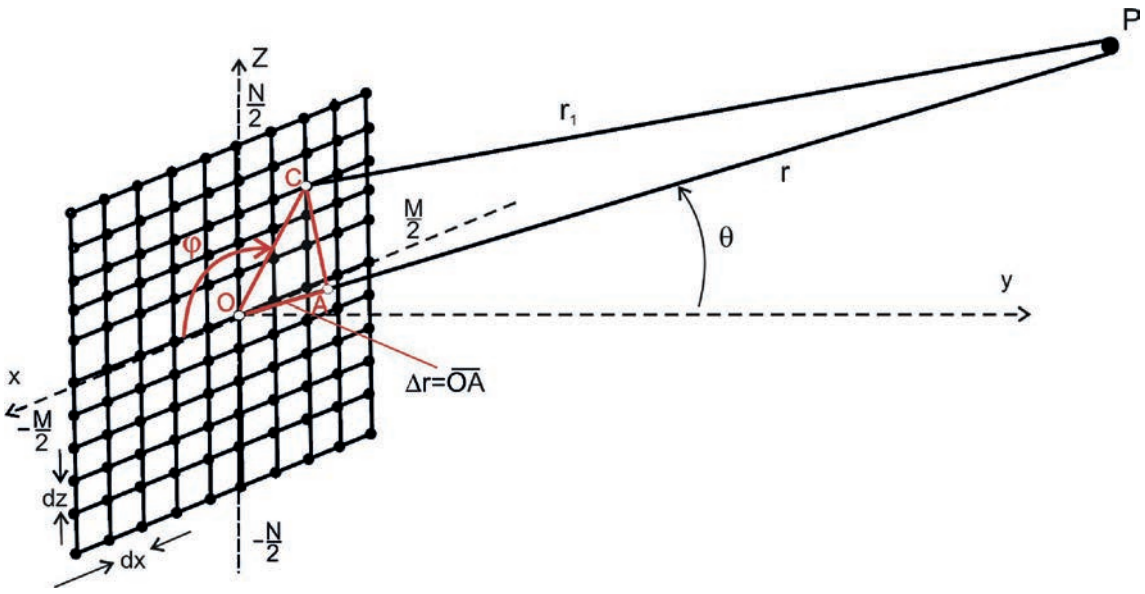

Fig. A2 - Geometric configuration of a planar array “discreet”.